

## Using [Ne V]/[Ne III] to Understand the Nature of Extreme-Ionization Galaxies

NIKKO J. CLERI,<sup>1,2</sup> GRACE M. OLIVIER,<sup>1,2</sup> TAYLOR A. HUTCHISON,<sup>3,\*</sup> CASEY PAPOVICH,<sup>1,2</sup> JONATHAN R. TRUMP,<sup>4</sup>  
RICARDO O. AMORÍN,<sup>5,6</sup> BREN E. BACKHAUS,<sup>4</sup> DANIELLE A. BERG,<sup>7</sup> VITAL FERNÁNDEZ,<sup>5</sup> STEVEN L. FINKELSTEIN,<sup>7</sup>  
SEIJI FUJIMOTO,<sup>8,9</sup> MICHAELA HIRSCHMANN,<sup>10</sup> JEYHAN S. KARTALTEPE,<sup>11</sup> DALE D. KOCEVSKI,<sup>12</sup> RAYMOND C. SIMONS,<sup>4</sup>  
STEPHEN M. WILKINS,<sup>13,14</sup> AND L. Y. AARON YUNG<sup>3,\*</sup>

<sup>1</sup>Department of Physics and Astronomy, Texas A&M University, College Station, TX, 77843-4242 USA

<sup>2</sup>George P. and Cynthia Woods Mitchell Institute for Fundamental Physics and Astronomy, Texas A&M University, College Station, TX, 77843-4242 USA

<sup>3</sup>Astrophysics Science Division, NASA Goddard Space Flight Center, 8800 Greenbelt Rd, Greenbelt, MD 20771, USA

<sup>4</sup>Department of Physics, 196 Auditorium Road, Unit 3046, University of Connecticut, Storrs, CT 06269

<sup>5</sup>Instituto de Investigación Multidisciplinar en Ciencia y Tecnología, Universidad de La Serena, Raul Bitrán 1305, La Serena 2204000, Chile

<sup>6</sup>Departamento de Astronomía, Universidad de La Serena, Av. Juan Cisternas 1200 Norte, La Serena 1720236, Chile

<sup>7</sup>Department of Astronomy, The University of Texas, Austin, Texas, 78712 USA

<sup>8</sup>Cosmic Dawn Center (DAWN), Jagtvej 128, DK2200 Copenhagen N, Denmark

<sup>9</sup>Niels Bohr Institute, University of Copenhagen, Lyngbyvej 2, DK2100 Copenhagen Ø, Denmark

<sup>10</sup>Institute of Physics, Laboratory of Galaxy Evolution, EPFL, Observatoire de Sauverny, 1290 Versoix, Switzerland

<sup>11</sup>Laboratory for Multiwavelength Astrophysics, School of Physics and Astronomy, Rochester Institute of Technology, 84 Lomb Memorial Drive, Rochester, NY 14623, USA

<sup>12</sup>Department of Physics and Astronomy, Colby College, Waterville, ME 04901, USA

<sup>13</sup>Astronomy Centre, University of Sussex, Falmer, Brighton BN1 9QH, UK

<sup>14</sup>Institute of Space Sciences and Astronomy, University of Malta, Msida MSD 2080, Malta

### ABSTRACT

Spectroscopic studies of extreme-ionization galaxies (EIGs) are critical to our understanding of exotic systems throughout cosmic time. These EIGs exhibit spectral features requiring  $>54.42$  eV photons: the energy needed to fully ionize helium into  $\text{He}^{2+}$  and emit He II recombination lines. Spectroscopic studies of EIGs can probe exotic stellar populations or accretion onto intermediate-mass black holes ( $\sim 10^2 - 10^5 M_\odot$ ), which are possibly key contributors to the reionization of the Universe. To facilitate the use of EIGs as probes of high-ionization systems, we focus on ratios constructed from several rest-frame UV/optical emission-lines:  $[\text{O III}]\lambda 5008$ ,  $\text{H}\beta$ ,  $[\text{Ne III}]\lambda 3870$ ,  $[\text{O II}]\lambda\lambda 3727, 3729$ , and  $[\text{Ne V}]\lambda 3427$ . These lines probe the relative intensity at energies of 35.12, 13.62, 40.96, 13.62, and 97.12 eV, respectively, covering a wider range of ionization than traced by other common rest-frame UV/optical techniques. We use ratios of these lines ( $[\text{Ne V}]/[\text{Ne III}] \equiv \text{Ne53}$ ,  $[\text{O III}]/\text{H}\beta$ , and  $[\text{Ne III}]/[\text{O II}]$ ) which are nearby in wavelength, mitigating effects of dust attenuation and uncertainties in flux calibration. We make predictions from photoionization models constructed from `CLOUDY` that use a broad range of stellar populations and black hole accretion models to explore the sensitivity of these line ratios to changes in the ionizing spectrum. We compare our models to observations from the *Hubble Space Telescope* and *James Webb Space Telescope* of galaxies with strong high-ionization emission lines at  $z \sim 0$ ,  $z \sim 2$ , and  $5 < z < 8.5$ . We show that the Ne53 ratio can separate galaxies with ionization from “normal” stellar populations from those with AGN and even “exotic” Population III models. We introduce new selection methods to identify galaxies with photoionization driven by Population III stars or intermediate-mass black hole accretion disks that could be identified in upcoming high-redshift spectroscopic surveys.

### 1. INTRODUCTION

Emission-line spectroscopy provides a wealth of information about the physical conditions of a galaxy. From a rest-

frame ultraviolet (UV)/optical spectrum of a galaxy, we can discern chemical abundances and metallicities (e.g., [Lequeux et al. 1979](#)), star formation rates (e.g., [Kennicutt 1998](#); [Kennicutt & Evans 2012](#)), nebular dust attenuation estimates (e.g., [Groves et al. 2012](#); [Buat et al. 2002](#)), temperatures and densities of the interstellar medium (ISM) (e.g., [Kewley et al. 2019](#); [Dopita et al. 2000](#); [Maiolino & Mannucci 2019](#)), and contributions of active galactic nuclei (AGN) to

Corresponding author: Nikko J. Cleri  
cleri@tamu.edu

\* NASA Postdoctoral Fellow

the emission (e.g., Baldwin et al. 1981; Veilleux & Osterbrock 1987; Trump et al. 2015). Much of the knowledge of these physical properties of a galaxy’s ionized gas is derived from bright Balmer lines of hydrogen ( $H\alpha$  and  $H\beta$ ), along with metal lines from oxygen ([O II]  $\lambda\lambda 3727, 3729$  and [O III]  $\lambda\lambda 4960, 5008$ ), sulfur ([S II]  $\lambda\lambda 6718, 6733$ ) and nitrogen ([N II]  $\lambda 6585$ )<sup>1</sup>, while P-cygni stellar wind features characterize the massive star population.

Historically, studies of emission-line galaxies use ratios of emission-line flux with small wavelength separations as a way to minimize uncertainties. Commonly-used emission-line ratios in the ultraviolet (UV) and optical such as [O III]  $\lambda 5008/H\beta$ , [Ne III]  $\lambda 3870/[O II] \lambda 3728$ , [N II]  $\lambda 6585/H\alpha$ , [S II]  $\lambda 6718/H\alpha$ , are relatively insensitive to dust attenuation and spectral calibrations, and as such are very useful tracers of ISM and AGN narrow-line region (NLR) conditions (e.g., Baldwin et al. 1981; Veilleux & Osterbrock 1987).

These rest-frame UV and optical emission-line ratios are tools for understanding how H-ionizing photons (Lyman continuum, LyC, photons of  $\lambda < 912 \text{ \AA}$ ) escaped from high-redshift galaxies. As such, this is paramount at  $z > 6$  as this radiation is the most likely candidate for reionizing the Universe (e.g., Finkelstein et al. 2015). Currently, few studies have successfully employed these UV and optical lines at  $z > 6$  during this so-called epoch of reionization (EoR), thus the physical nature of the ionizing spectra and physical properties of the galaxies responsible remain poorly understood. With the advent of the *James Webb Space Telescope* (*JWST*) era, we now have unprecedented access to spectroscopic observations of these early-Universe systems. The Near-Infrared Spectrograph (*JWST*/NIRSpec) coverage spans  $0.6\text{--}5.3 \mu\text{m}$ , allowing detection of rest-frame UV and optical emission lines well into the EoR, with spectral resolutions ( $R \sim 1000$  or  $R \sim 2700$  depending on the observing mode) easily capable of resolving important emission features for these studies.

The chemically young and highly energetic stellar populations in galaxies during the EoR are expected to be key contributors to the hydrogen reionization of the Universe (e.g., Berg et al. 2016, 2019, 2021; Finkelstein et al. 2015; Curtis-Lake et al. 2023; Trump et al. 2023; Brinchmann 2023; Zackrisson et al. 2011; Trussler et al. 2022). These objects show prominent high-ionization ( $\gtrsim 35 \text{ eV}$  creation potential, Berg et al. 2021) emission lines, suggesting that they are characterized by hard radiation fields (Smit et al. 2014; Stark 2016; Trump et al. 2023; Brinchmann 2023; Katz et al. 2023).

Previous studies of high-ionization emission-line galaxies (ELGs) have focused primarily on spectral features in

the Berg et al. (2021) “high-ionization regime”, including C IV  $\lambda\lambda 1548, 1551$ , [Ne III]  $\lambda 3870$ , [O III]  $\lambda\lambda 4960, 5008$ , He II  $\lambda 1640$ , He II  $\lambda 4687$ , and [Ar IV]  $\lambda\lambda 4712, 4741$  (e.g., Berg et al. 2016, 2019, 2021; Olivier et al. 2022; Levesque & Richardson 2014; Masters et al. 2014; Zeimann et al. 2015; Backhaus et al. 2022; Atek et al. 2011; van der Wel et al. 2011; Maseda et al. 2013, 2014; Tang et al. 2019, 2021; Senchyna et al. 2017, 2020; Rigby et al. 2015; Kehrig et al. 2015, 2018, 2021; Amorín et al. 2015, 2017; Pérez-Montero et al. 2021). Several studies have already suggested that chemically-evolved Population I and II stars are unable to account for the strength of emission in the highest-energy lines, and instead they require additional sources of (hard) ionizing spectra (e.g., Steidel et al. 2014; Olivier et al. 2022).

Such systems, which we dub “extreme-ionization galaxies” (EIGs), exhibit spectral features which require radiation hard enough to fully ionize helium ( $> 54.42 \text{ eV}$ ). These galaxies often require harder ionization than produced from “normal” stellar populations to produce such high-energy emission features. Such ionizing sources may be more exotic than “normal” stellar populations, including accreting massive black holes, supernovae, Population III stars, Wolf-Rayet stars, stripped stars in binaries, high-mass X-ray binaries (HMXBs), hot, low-mass evolved stars (HOLMES, Flores-Fajardo et al. 2011). Features seen in spectra of EIGs may include lines from helium (e.g., He II  $\lambda 1640$ , He II  $\lambda 4687$ ), nitrogen (e.g., N V  $\lambda\lambda 1240, 1244$ ), oxygen (e.g., O IV]  $\lambda\lambda 1401, 1405$ ), neon (e.g., [Ne IV]  $\lambda 2423$ , [Ne V]  $\lambda\lambda 3347, 3427$ ), iron (e.g., [Fe X]  $\lambda 6375$ ), and many others. These conditions appear indicative of rapidly accreting black holes or low-metallicity, recently formed stellar populations. We expect these conditions to be more apparent at higher redshifts, particularly in the EoR. Early work with *JWST* suggests that many EoR galaxies have metallicities of  $\sim 5\text{--}10\%$   $Z_{\odot}$  (e.g., Trump et al. 2023; Brinchmann 2023), and have also suggested the existence of active black hole accretion in the very early Universe (e.g., Brinchmann 2023; Larson et al. 2023; Maiolino et al. 2023). In light of these recent results, it is prudent to consider the conditions that could produce EIGs at these early epochs.

In this work, we focus on emission in EIGs from quadruply-ionized neon through [Ne V]  $\lambda 3427$ <sup>2</sup> (vacuum wavelength) and its ratios with other bright UV/optical lines.

The ionization energy needed to produce  $\text{Ne}^{4+}$  ( $97.11 \text{ eV}$ ) is extremely high compared to most other strong UV/optical emission lines; [Ne V] emission requires energies nearly

<sup>1</sup> Vacuum wavelengths

<sup>2</sup> The near-UV/optical [Ne V] is a doublet with lines at  $3427 \text{ \AA}$  and  $3347 \text{ \AA}$ . However, the  $3347 \text{ \AA}$  line is weaker (with a typical ratio of 2.73:1 for [Ne V]  $\lambda 3427/[Ne V] \lambda 3347$ ) and the [Ne V]  $\lambda 3347$  line can be blended with other nearby lines (see Section 4.2 for more discussion). We therefore focus on [Ne V]  $\lambda 3427$  in this work.

triple that of [O III] (35.12 eV), more than double that of [Ne III] (40.96 eV), and nearly double that of He II (54.42 eV). This property places [Ne V] well above the lower bound of the [Berg et al. \(2021\)](#) “very high” ionization zone, and as such probes a parameter space of the ISM not traced by other strong UV/optical lines<sup>3</sup>

The production of high-ionization emission lines such as [Ne V] requires an extremely hard photoionizing source. Previous works have attributed [Ne V] production to photoionization from active galactic nuclei (AGN), stellar continuum from an extremely hot ionizing spectrum including Wolf-Rayet stars, or energetic radiative shocks from supernovae ([Zeimann et al. 2015](#); [Backhaus et al. 2022](#); [Gilli et al. 2010](#); [Mignoli et al. 2013](#); [Izotov et al. 2012](#); [Cleri et al. 2023](#)).

AGN, produced from accretion onto black holes (BHs), are clear candidates for production of photons needed to produce high-ionization emission lines.<sup>4</sup> Previous works have studied [Ne V] and its correlations with X-ray luminosities in local Seyferts and low-redshift ( $z < 1.5$ ) quasi-stellar objects (QSOs) ([Gilli et al. 2010](#); [Mignoli et al. 2013](#)). Accretion onto intermediate-mass black holes (IMBHs) has remained an open field of study, though models predict that the accretion disks around IMBHs ( $\log(M_{\text{BH}}/M_{\odot}) \lesssim 5$ ) produce harder radiation fields than their supermassive counterparts ([Done et al. 2012](#)). These lower-mass accretion disk models are predicted to emit photons hard enough to produce very-high-ionization ( $>54.42$  eV) emission features ([Cann et al. 2018](#)).

Around the peak of cosmic star formation rate density and AGN activity at  $z \sim 1-2$ , studies have found that [Ne V] emission is consistent with photoionization from AGN ([Cleri et al. 2023](#); [Backhaus et al. 2022](#)). [Cleri et al. \(2023\)](#) finds that [Ne V]-emitting galaxies at these redshifts are five times more likely to be X-ray confirmed AGN than galaxies without [Ne V]-detections, and that a majority (88%) of their objects are consistent with AGN emission in optical [Baldwin et al. 1981](#) (BPT)-like emission-line ratio diagnostics.

Some studies of local ( $z \sim 0$ ) low-mass ( $\log M_*/M_{\odot} \lesssim 8$ ), star-forming (SF) galaxies have explained [Ne V] production through energetic supernova shocks. [Izotov et al. \(2012\)](#) finds five oxygen-poor blue compact dwarf (BCDs) galaxies with [Ne V] emission which have [Ne V]/He II flux ratios reproducible by radiative shock models with shock velocities

in the 300-500 km s<sup>-1</sup> range and shock ionizing contributions that are  $\sim 10\%$  of that from the stellar continuum ionization. However, this modeling cannot conclusively rule out that this  $\sim 10\%$  contribution of the [Ne V] emission comes from AGN. These studies have primarily focused on low-mass galaxies (BCDs in the case of [Izotov et al. 2012](#)), so it is unclear if shocks can account for [Ne V] emission in more massive galaxies that dominate the peak of cosmic star formation rate density. Alternatively, [Olivier et al. 2022](#) has attributed local [Ne V] production to young ( $\sim 5$  Myr) extremely metal-poor ( $Z \lesssim 0.1Z_{\odot}$ ) bursts of star formation plus an additional very hot ionizing source, modeled by an 80-100 kK blackbody (in excess of what is available in “normal” Population I or II stellar populations).

Another intriguing engine for the energetic photons required to produce [Ne V] is the exotic stellar populations in the very early Universe. Population III (Pop III) stars were likely very massive ( $>50 M_{\odot}$ , [Zackrisson et al. 2011](#)), with mass upper limits possibly even as great as  $1000 M_{\odot}$  ([Bromm et al. 1999](#); [Nakamura & Umemura 2002](#); [Tan & McKee 2004](#); [Greif & Bromm 2006](#); [Ohkubo et al. 2009](#)). Such chemically young populations likely initiated the metal enrichment of the succeeding generations of “normal” Population I and II stars in the later Universe ([Heger et al. 2002](#)). While truly primordial gas would not show metal emission, the chemical enrichment of the ISM of early galaxies occurs rapidly given the short lifetimes of Pop III stars ([Finlator et al. 2015, 2016, 2018](#)). However, the short lifetimes of these Pop III stars introduces another complication; observation of high-ionization metal emission lines from the newly-enriched ISM requires very recent ( $\lesssim 1$  Myr) star formation for such short-lived stars.

The spectral energy distributions (SEDs) of these Pop III stars are most likely to peak in the extreme-UV ( $<912$  Å), around the energies needed to fully ionize helium at 54.42 eV ([Zackrisson et al. 2011](#); [Schaerer 2002](#); [Trussler et al. 2022](#)). Stellar population synthesis codes predict that the SEDs of these Pop III stars may produce photons at even higher energies, even into to very soft X-ray regime (e.g. see the Yggdrasil models of [Zackrisson et al. 2011](#); [Trussler et al. 2022](#)). This would allow for production of ultra high-ionization emission lines like [Ne V] to be powered solely from these primordial stars provided the nebula ionized by these stars contains *some* elements heavier than He.

We can alleviate the potential degeneracies between Pop III stars and other high-ionization sources (e.g., AGN, supernova shocks, Wolf-Rayet stars, high-mass X-ray binaries) with deeper information from the rest-frame UV/optical spectra. The UV continuum can be used to derive the metallicity of the stellar populations, and the gas-phase metallicity can be derived from emission features. Other ionizing engines such as AGN, supernova shocks, and Wolf-Rayet stars

<sup>3</sup> The  $\gtrsim 100$  eV energy regime also ionizes both hydrogen and helium to produce H I and He II photons; however, the minimum energy required to produce He II emission (54.42 eV) and H I emission (13.6 eV) is a factor of  $\sim 2-7$  lower than that of [Ne V] (97.11 eV).

<sup>4</sup> Here we use “Active Galactic Nuclei” (AGN) to indicate radiation from any accreting black hole. This includes both AGN associated with supermassive black holes ( $M_{\text{BH}} \gtrsim 10^6 M_{\odot}$ ) and AGN arising from accretion onto more modest “intermediate” mass black holes (IMBHs) with  $M_{\text{BH}} \lesssim 5 M_{\odot}$ , see e.g., [Cann et al. \(2018\)](#).

can produce broader emission features than standard HII regions, and X-ray observations can rule out high-mass X-ray binaries (e.g., [Senchyna et al. 2020](#)).

For objects which are not deeply observed across all wavelengths, separating photoionization from Pop III stars and AGN or other sources is often difficult (e.g., [Katz et al. 2022](#)). Several works have offered potential solutions in the form of emission line ratios of high-ionization to low-ionization lines (such as He II/H $\beta$ ), in conjunction with derived gas-phase metallicities (e.g., [Schaerer 2002](#); [Raiter et al. 2010](#); [Inoue 2011](#); [Katz et al. 2022](#); [Trussler et al. 2022](#)).

In this work, we offer a potential diagnostic for photoionization from stellar populations or black hole accretion disks using a combination of rest-frame UV/optical emission line ratios ([O III]/H $\beta$ , [Ne III]/[O II], [Ne V]/[Ne III]). These line ratios are closely spaced in wavelength, and can be observed out to  $z \sim 9$  in upcoming spectroscopic surveys at high-redshifts with *JWST*.

The outline of this work is as follows: Section 2 describes our photoionization models. Section 3 describes our comparison samples. Section 4 compares UV/optical emission-line ratios as diagnostics of AGN activity. Section 5 discusses the implications of our results. Section 6 summarizes the results of this work and discusses future studies of high-ionization galaxies with *JWST*.

## 2. PHOTOIONIZATION MODELS

To explore the physical conditions of EIGs throughout cosmic time, we employ photoionization modeling of local stellar populations, black hole accretion disks, and Pop III stars. For the following analysis, we use *Cloudy* version C17.01 ([Ferland et al. 2017](#)). *Cloudy* is a photoionization simulation code designed to self-consistently model physical conditions in astrophysical clouds to predict thermal, ionization, and chemical structure of the cloud and predict its observed spectrum.

Our models assume a hydrogen density of  $10^2 \text{ cm}^{-3}$ , with the *Cloudy* default [Grevesse et al. \(2010\)](#) solar abundance ratios and Orion dust grains for the initial gas phase and dust abundances. The emissivity of [Ne V]/[Ne III] is relatively insensitive to fluctuations in density (see Appendix B of [Cleri et al. 2023](#)). Unless otherwise stated, we assume a plane-parallel gas geometry for all models.

We run all of our models across a grid of ionization parameters<sup>5</sup> from  $-4 < \log U < -1$  in steps of 0.25, where  $U = q/c$  is the dimensionless ionization parameter. [Kewley et al. \(2019\)](#) defines the dimensionless ionization parameter

as

$$U \equiv \frac{1}{c} \frac{\Phi}{n_H} \quad (1)$$

where  $\Phi$  is the ionizing photon flux and  $n_H$  is the hydrogen density.

The details of the individual models used in this work are described in the following subsections.

### 2.1. “Normal” Stellar Population Models

The stellar population models used in this work are from the Binary Population and Spectral Synthesis (BPASS; v2.2.1) single-burst binary-formation library ([Stanway & Eldridge 2018](#)). The BPASS-only models use an IMF with a [Salpeter 1955](#) slope ( $\alpha = -2.35$ ) for all masses, and an upper mass limit of  $100 M_\odot$ . Unless otherwise stated, we use a single-burst stellar population with an age of 3 Myr, with stellar metallicities in a grid of  $Z = 0.00005, 0.05, 0.10, 0.20, 0.50, 1.0 Z_\odot$ . We note that  $Z = 0.05 Z_\odot$  gas-phase metallicity is consistent with extremely metal-poor dwarf galaxies ( $Z < 0.1 Z_\odot$ ) in the local Universe, and recent *JWST* spectra have not derived lower gas-phase metallicities than 5% solar ([Olivier et al. 2022](#); [Berg et al. 2019, 2021](#); [Trump et al. 2023](#); [Brinchmann 2023](#)). We also use a composite stellar population model that adds to BPASS models a hot (80 kK) blackbody needed to reproduce emission from very-high-ionization lines such as He II and C IV from [Olivier et al. 2022](#) (see Section 3.1).

### 2.2. “Exotic” Population III Star Models

To test exotic stellar populations potentially found in the early Universe, we also employ models of Pop III stars from the Yggdrasil population synthesis code ([Zackrisson et al. 2011](#)). We use the Pop III.1 model with a zero-metallicity population with an extremely top heavy IMF ( $50\text{--}500 M_\odot$ ) and a [Salpeter \(1955\)](#) slope ( $\alpha = -2.35$ ) for all masses, with a single stellar population (SSP) from [Schaerer \(2002\)](#). We also use the Yggdrasil Pop III.2 model, which is also a zero-metallicity stellar population but with a more moderately top-heavy IMF: log-normal with characteristic mass  $M_c = 10 M_\odot$ , dispersion  $\sigma = 1 M_\odot$ , extending from  $1\text{--}500 M_\odot$  ([Raiter et al. 2010](#); [Tumlinson 2006](#)).

For these models, the stellar population is assumed to have zero metallicity, but we employ a (slightly) enriched gas-phase metallicity of  $Z = 0.05 Z_\odot$ . For the very first population of stars, the gas-phase metallicity would be effectively null; this would yield no metal emission features, i.e., only hydrogen and helium emission. We assume that there must be some chemical enrichment in the ISM from primordial supernovae or stellar mass loss events for metals to be present. This 5% solar gas-phase metallicity is consistent with extremely metal-poor dwarf galaxies in the local Universe, the

<sup>5</sup> This is the initial ionization parameter *Cloudy* assumes at the incident face of the cloud.



most likely well-studied analogs to these high-redshift systems (e.g., [Berg et al. 2016, 2019, 2021](#); [Olivier et al. 2022](#)).

### 2.3. Black Hole Accretion Models

Accretion onto BHs offers another source of high energy photons that are capable of [Ne V] production. We tested both theoretical models for accretion onto black holes, as well as empirical models for active galactic nuclei (AGN).

The theoretical models for black hole accretion are based on SEDs from [Done et al. \(2012\)](#). These models include a blackbody disk as well as a Compton upscattering component from the disk to recreate the “soft X-ray excess” often observed in AGN in the local Universe (e.g., [Done et al. 2012](#); [Gierliński & Done 2004](#); [Walter & Fink 1993](#)). The final component to this model is a power-law tail to model the high energy emission which is the result of a second Compton upscattering that takes place in the optically thin corona above the disk. The [Done et al. \(2012\)](#) models are available from XSPEC ([Arnaud 1996](#)) using the OPTXAGNF command. We produce SEDs of black holes with masses from  $10^3$ – $10^8 M_\odot$  and keep the parameters as the default parameters for this model except for the electron temperature associated with the soft Comptonization component which we set to 0.1 keV instead of the default 0.2 keV as this is more similar to the models used by [Cann et al. \(2018\)](#).

Given the intricacies of accurately modeling black hole accretion disk physics, the models used in this work are relatively simplistic ([Adhikari et al. 2016](#); [Mitchell et al. 2023](#)). They employ a single cloud to represent the broad-line and narrow-line regions, among other simplifications ([Cann et al. 2018](#)). More sophisticated models are an active area of work (e.g., [Mckaign et al. in prep.](#)). Potential improvements to these models include separate BLR and NLR physics, as well as other updates. These updated models are not likely to have a significant impact on the parameter space of interest in this work (i.e.,  $\lesssim 100$  eV emission lines), but will include significant improvements at higher energies ([Mckaign & Satyapal, private communication](#)).

We derive the gas-phase metallicities for these black hole accretion disk models from the mass-metallicity relation of [Papovich et al. \(2022\)](#). We derive respective stellar masses for the galaxies surrounding these black hole accretion disks using the [Kormendy & Ho 2013](#) scaling relations. The [Papovich et al. 2022](#) mass-metallicity relation is calibrated for more massive ( $\gtrsim 10^9 M_\odot$ ) ELGs around the peak of cosmic star formation rate density and AGN activity at  $z \sim 1$ – $2$ , so we extrapolate the relation for the  $M_{\text{BH}} \leq 10^5 M_\odot$ , and set a minimum gas-phase metallicity for our lowest black hole mass models of  $Z = 0.05 Z_\odot$ .

To probe a representative of the AGN parameter space with a well-studied local active galaxy, we also include the SED of the nearby Seyfert 1 galaxy NGC 5548 ([Mehdipour et al.](#)

[2015](#)). NGC 5548 has a multiwavelength SED from near-infrared to the hard (200 keV) X-ray. The UV to near-IR continuum of NGC 5548 is consistent with being composed of a single Comptonized disk component, with no evidence of an additional purely-thermal disk component or additional component of reprocessing from the disk. Notably, NGC 5548 also exhibits a “soft X-ray excess”, which is correlated with the production of photons required to ionize neon to produce [Ne V]. NGC 5548 has a central engine powered by a  $6.5 \times 10^7 M_\odot$  supermassive black hole ([Bentz et al. 2007](#)).

Several works suggest other empirical SED shapes for low-redshift Seyferts ([Binette et al. 1989](#); [Clavel et al. 1990](#)) or high-redshift quasars ([Zheng et al. 1997](#); [Korista et al. 1997](#); [Vanden Berk et al. 2001](#); [Richards et al. 2006](#); [Fan et al. 2006](#)), yet these models are similar in shape to the [Done et al. 2012](#) SEDs. Ultimately, the nature of AGN SEDs remains an open question, especially for the low-mass and low-luminosity regimes. Lower-mass accreting black holes ( $\lesssim 10^5 M_\odot$ ) may be key contributors to the high-ionization photon production of the early Universe, yet remain poorly understood.

### 2.4. SEDs and Cloudy Output Spectra

Our photoionization models for black hole accretion and stellar populations produce a wide range of emission at different energies. Figure 1 shows these input SEDs used in our photoionization models. These include: (1) a 3 Myr BPASS stellar population with continuum and gas-phase metallicity  $0.05 Z_\odot$ ; (2) a model that includes the 3 Myr BPASS stellar population with an additional 80 kK black body (needed to reproduce line ratios seen in the  $z \sim 0$  metal-poor dwarf galaxy J141851; [Olivier et al. 2022](#), see Section 3.1 for details); (3) the [Done et al. 2012](#) black hole accretion disk models for black hole masses ranging from  $\log M_{\text{BH}}/M_\odot = 4$  to  $\log M_{\text{BH}}/M_\odot = 8$ ; (4) the [Mehdipour et al. 2015](#) NGC 5548 SED, and (5) the Yggdrasil Pop III.1 and III.2 SEDs. All of the models shown in Figure 1 are normalized at 1500 Å. We mark the four ionization zones of [Berg et al. \(2021\)](#):

1. Low Ionization: Energy needed to produce  $\text{N}^+$  (14.53–29.60 eV)
2. Intermediate Ionization: Energy needed to produce  $\text{S}^{2+}$  (23.33–34.79 eV)
3. High Ionization: Energy needed to produce  $\text{O}^{2+}$  (35.11–54.93 eV)
4. Very High Ionization: Energy needed to produce  $\text{He}^{2+}$  (>54.42 eV)

Figure 2 shows the rest-frame NUV/optical Cloudy output intrinsic spectra from the respective ionizing SEDs in Figure 1. We mark several lines of interest:

[Ne V]  $\lambda\lambda 3347, 3427$ , [O II]  $\lambda\lambda 3727, 3729$ , [Ne III]  $\lambda 3870$ , He II  $\lambda 4687$ , H $\beta$ , and [O III]  $\lambda\lambda 4960, 5008$ . We note that there is a large apparent difference between the spectra at the wavelengths of the [Ne V] lines. There is clear emission of [Ne V] in the AGN, NGC 5548, Pop III.1, and Pop III.2 spectra, but minimal [Ne V] in the BPASS 3 Myr or [Olivier et al. \(2022\)](#) BPASS+blackbody spectra. For visualization purposes, we smooth the Cloudy emission lines into Gaussians. We assume wind speeds of 250 km/s for the BPASS models and the [Olivier et al. 2022](#) BPASS+blackbody models (see [Olivier et al. 2022](#) for details), 460 km/s for the black hole accretion disk models and NGC 5548 ([Peterson et al. 2013](#)). For the Yggdrasil Pop III models, we assume minimal 100 km/s winds; winds are metal driven, so true first-population stars will have zero wind (e.g., [Schaerer 2002](#); [Kudritzki 2000](#); [Baraffe & Kolb 2000](#)). The default spectral resolution of Cloudy is  $R = 300$ , so we note that there will be blending issues with other lines in the output spectra; as such, this Gaussian smoothing should be used only for visualization purposes.

### 3. DATA

We compare our models to galaxies at  $z \sim 0$  from [Berg et al. \(2021\)](#) and [Olivier et al. \(2022\)](#),  $z \sim 1.6$  from [Cléri et al. \(2023\)](#), and  $5 < z < 8.5$  from [Trump et al. \(2023\)](#), where for the latter we have made new measurements of [Ne V] as part of this work. We briefly describe these observations in the following subsections.

#### 3.1. Observations at $z \sim 0$

We compare our models with two galaxies in the nearby Universe which exhibit exceptional extreme emission-line behavior. These objects have been studied in detail in [Berg et al. \(2016, 2019, 2021\)](#); [Olivier et al. \(2022\)](#):

- J104457 has the largest C IV  $\lambda\lambda 1548, 1550$  Å equivalent width ( $-6.71$  Å,  $-2.83$  Å<sup>6</sup>) measured in the local Universe.
- J141851 has the largest He II  $\lambda 1640$  Å equivalent width ( $-2.82$  Å) measured in the local Universe.

J104457 and J141851 have far-UV spectra taken with the Cosmic Origins Spectrograph (COS) on *HST* (*HST* Proposal ID 15465) and near-UV/Optical spectra from the Multi-Object Double Spectrograph (MODS) on the Large Binocular Telescope (LBT). They are both extremely metal-poor dwarf galaxies with derived gas-phase metallicities of 5.8% and 8.7% solar, respectively, and low stellar masses of  $\log M_*/M_\odot = 6.80$  and 6.63, respectively.

<sup>6</sup> Negative equivalent widths indicate emission features.

#### 3.1.1. Stellar Population + Blackbody Models

We also employ photoionization models used by [Olivier et al. \(2022\)](#) to reproduce the emission line strengths in two galaxies, J104457 and J141851. These models add (very hot) blackbodies to BPASS stellar populations in order to reproduce the emission of high-ionization spectral features such as C IV, and He II. [Olivier et al. \(2022\)](#) matches physical conditions of the galaxies (densities, abundances, etc.) and the full suite of low- to very-high-ionization lines in the rest-frame far-UV to optical to constrain the full shape of the ionizing spectra. They find that the models which best reproduce the very-high-ionization emission in their galaxy J141851 (see Section 3.1) are those with stellar contributions from BPASS contributing 45% of the total luminosity, along with an injected 80 kK blackbody contributing the remaining 55% of the total luminosity (see discussion in the next paragraph). These models use BPASS stellar populations with an IMF with low-mass ( $< 0.5M_\odot$ ) slope  $\alpha = -1.3$ , and high-mass ( $> 0.5M_\odot$ ) slope  $\alpha = -2.35$ , with upper mass limit  $100M_\odot$  (see Section 3 in [Olivier et al. 2022](#)).

[Olivier et al. \(2022\)](#) found that the ionizing spectra of J104457 and J141851 are consistent with extremely metal-poor stellar populations as represented by this extreme model that requires the addition of a hard photoionizing source, represented by this 80 kK blackbody, in order to produce the very-high-ionization lines. The physical origin of this hard photoionizing source is unknown, but could be a result of high-mass binaries, supersoft X-ray sources, stripped stars and Wolf-Rayet stars, or a combination of these or other exotic populations (see [Olivier et al. 2022](#) for a full discussion).

The two models from galaxies J104457 and J141851 take the derived gas-phase metallicities of 5.8% and 8.7% solar, respectively. They assume a spherical cloud and scale nitrogen and carbon in the gas by their measured abundances (see [Olivier et al. 2022](#) for more details).

#### 3.2. Observations at $z \sim 1.6$

The [Cléri et al. \(2023\)](#) sample of [Ne V]-emitting galaxies is selected from the CLEAR ([Estrada-Carpenter et al. 2019, 2020](#); [Simons et al. 2021, 2023](#)) parent catalog of *HST*/Wide Field Camera 3 (WFC3) G102 and G141 grism observations using the following selection criteria:

- Require a grism spectroscopic redshift,  $1.39 < z < 2.30$ , such that both [Ne V] and [O III] are within the observed-frame spectral range of G102 and G141 sensitivity (0.8-1.65  $\mu\text{m}$ ).
- Require signal-to-noise ratio (S/N) of at least 3 for [Ne V]  $\lambda 3427$  and [O III]  $\lambda\lambda 4960, 5008$ .
- Visual inspection of direct images with 1D and 2D spectra to ensure that no objects with poor continuum

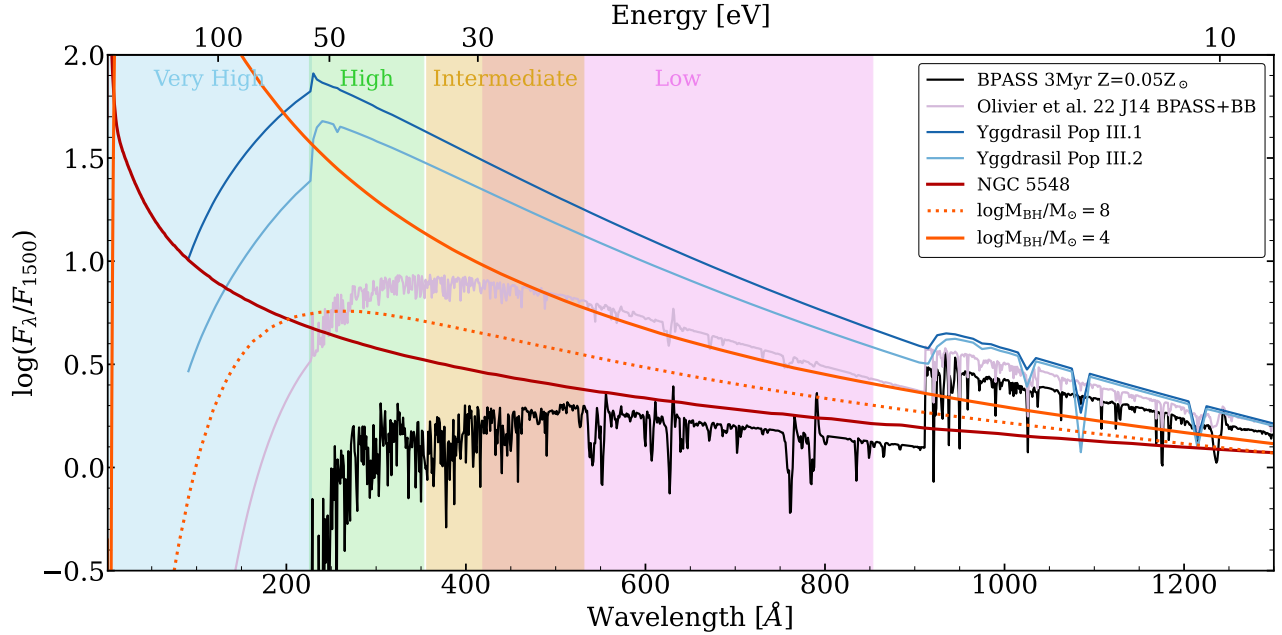


**Figure 1.** Example input SEDs of the various models used in our photoionization modeling. We show a pure BPASS 5% solar 3 Myr stellar population model in black, the [Olivier et al. \(2022\)](#) BPASS+blackbody model for J141851 in purple, the black hole accretion disk models in orange ( $\log M_{\text{BH}}/M_{\odot} = 8$  dotted,  $\log M_{\text{BH}}/M_{\odot} = 4$  solid), NGC 5548 in red, and the Yggdrasil Pop III.1 and III.2 models in dark and light blue, respectively. All models are normalized in  $F_{\lambda}$  at 1500 Å. The shaded regions mark the four zones of ionization from [Berg et al. \(2021\)](#) (see Section 2).

modeling and/or bad contamination subtraction make it into the final selection.

This selection leaves 25 galaxies with significant [Ne V] emission. See [Cleri et al. \(2023\)](#) for further details on the individual steps of the sample selection.

### 3.3. Observations at $5 < z < 8.5$

To test our models against galaxies in the epoch of reionization, we use the [Trump et al. \(2023\)](#) sample. This sample contains five galaxies at  $5.2 < z < 8.5$  from *JWST*/NIRSpec observations of the SMACS 0723 Early Release Observations ([Pontoppidan et al. 2022](#)). Each galaxy was observed with NIRSpec in two visits (s007 and s008, see [Trump et al. 2023](#)).

The [Trump et al. \(2023\)](#) results include measurements for several emission lines of interest: [O II]  $\lambda\lambda 3727, 3729$ , [Ne III]  $\lambda 3870$ , [O III]  $\lambda 4364$ ,  $H\gamma$ , He II  $\lambda 4687$ ,  $H\beta$ , [O III]  $\lambda 4960$ , and [O III]  $\lambda 5008$ . In this work, we have refit the galaxies from the [Trump et al. \(2023\)](#) sample to probe for emission from [Ne V]  $\lambda 3427$ . In three of the five sources we find possible detections of [Ne V] with S/N 1-3. Of the two remaining galaxies, one shows no evidence of [Ne V] emission (S/N < 1). In the remaining galaxy, (ID 5144 in the catalog of [Trump et al.](#)), the [Ne V]  $\lambda 3427$  line is not covered as its wavelength falls in a detector gap in the NIRSpec gratings. Figure 3 shows fits to the emission in the region of [Ne V] for the four galaxies with coverage. The detections of [Ne V] are

marginal ( $1 \lesssim \text{S/N} \lesssim 3$ ) at best, but we include them as useful upper limits in our analysis below. We report the S/N ratios of the relevant emission lines as well as the [Ne V]/[Ne III] limits (see Section 4.2), [Ne III]/[O II], and [O III]/ $H\beta$  ratios and their uncertainties in Table 1. All of the values presented in Table 1 are for the coadded spectra between the two visits. [Ne V]  $\lambda 3427$  cannot be measured for ID 5144 as [Ne V] lies in a detector gap at this redshift. There is also a spectral artifact in the region of [Ne V]  $\lambda 3427$  in one visit of ID 8140.

## 4. EMISSION-LINE RATIO CLASSIFICATIONS OF STELLAR POPULATIONS AND AGN

### 4.1. The OHNO Diagram

The OHNO ([O III]/ $H\beta$  and [Ne III]/[O II]) diagram ([Zeimann et al. 2015](#); [Backhaus et al. 2022](#)) is an emission-line ratio diagnostic designed to separate star-forming galaxies from AGN around  $z \sim 2$ . This diagnostic compares ratios of emission lines at similar wavelengths ([O II]  $\lambda\lambda 3727, 3729$ , [Ne III]  $\lambda 3870$ ,  $H\beta$ , and [O III]  $\lambda\lambda 4960, 5008$ ) where the production of [O III] and [Ne III] both require higher photon energies: the first two ionization energies of oxygen (the minimum energies required to produce [O II] and [O III] photons) are 13.62 eV and 35.12 eV, and the second ionization energy of neon (the minimum energy required to produce [Ne III] photons) is 40.96 eV. Galaxies with strong [O III]/ $H\beta$  and/or [Ne III]/[O II] require harder radiation fields, typically found in the emission-line

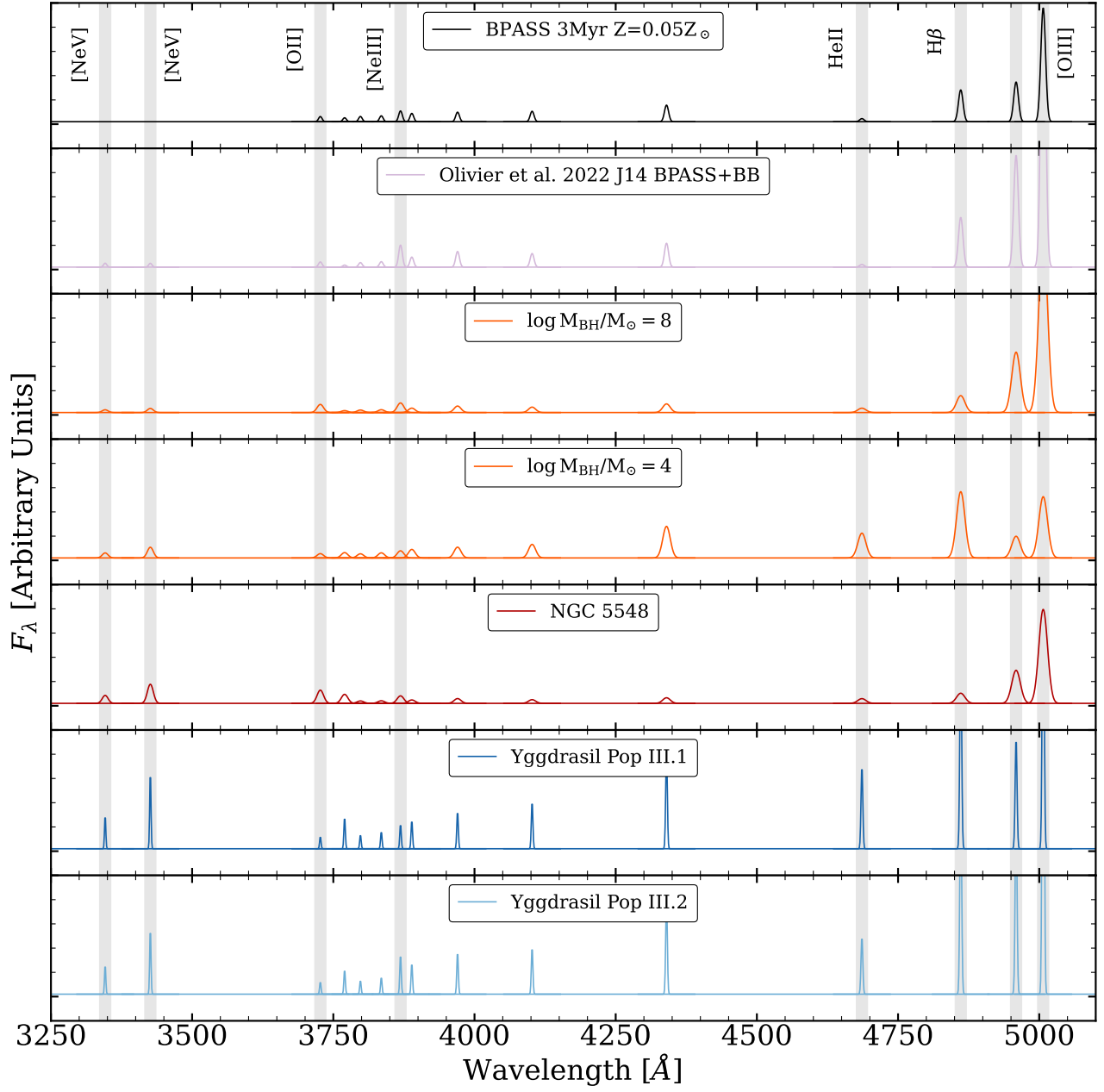


**Figure 2.** Example `Cloudy` output spectra of the various models used in this work. We show a pure BPASS 5%  $Z_{\odot}$  3 Myr stellar population model in black, the [Olivier et al. \(2022\)](#) BPASS+blackbody model for J141851 in purple, the black hole accretion disk models in orange ( $\log M_{\text{BH}}/M_{\odot} = 8$  and  $\log M_{\text{BH}}/M_{\odot} = 4$ ), NGC 5548 in red, and the Yggdrasil Pop III.1 and III.2 models in dark and light blue, respectively. We note several lines of interest: [Ne V]  $\lambda\lambda 3347, 3427$ , [O II]  $\lambda\lambda 3727, 3729$ , [Ne III]  $\lambda 3870$ , He II  $\lambda 4687$ , H $\beta$ , [O III]  $\lambda\lambda 4960, 5008$ . For visualization purposes, we smooth the `Cloudy` spectra into Gaussians for each emission line (see Section 2 for details).

regions of AGN. [Backhaus et al. \(2022\)](#) showed that division in the OHNO line ratios separates X-ray–selected AGN from non-AGN (based on classifications from the deep X-ray data in the Chandra Deep Fields at  $z \sim 1$ ). [Backhaus et al. \(2022\)](#) defines the OHNO star-formation/AGN dividing line as

$$\log \left( \frac{[\text{O III}]}{\text{H}\beta} \right) = \frac{0.35}{2.8 \log([\text{Ne III}]/[\text{O II}]) - 0.8} + 0.64 \quad (2)$$

The OHNO diagnostic has also been used to show that [Ne V]-emitting galaxies near the peak of cosmic star formation and AGN activity at  $z \sim 1-2$  are preferentially classified as AGN ([Backhaus et al. 2022](#); [Cleri et al. 2023](#)).

At high redshifts, it becomes difficult to distinguish between galaxies with photoionization from stellar populations and those with AGN using only OHNO. We show the OHNO diagram in Figure 4. We also show our stellar,



**Table 1.** Measurements from NIRSpec data on SMACS Galaxies

ID	Redshift	[Ne V] $\lambda 3427$ <sup>i</sup>	[O II] $\lambda\lambda 3727, 3729$ <sup>i</sup>	[Ne III] $\lambda 3870$ <sup>i</sup>	H $\beta$ <sup>i</sup>	[O III] $\lambda 5008$ <sup>i</sup>	[Ne V]/[Ne III] <sup>ii</sup>	[Ne III]/[O II]	[O III] $\lambda 5008$ /H $\beta$
4590	8.4957	2.3	3.2	6.8	20.4	38.3	<0.61	$1.82 \pm 0.63$	$3.05 \pm 0.17$
5144	6.3792	...	7.4	10.8	27.4	86.3	...	$1.32 \pm 0.22$	$6.45 \pm 0.25$
6355	7.6651	1.8	23.5	15.5	26.3	96.5	<0.20	$0.48 \pm 0.04$	$8.23 \pm 0.32$
8140	5.2753	0.4	13.7	4.6	6.9	28.6	<0.44	$0.39 \pm 0.09$	$6.82 \pm 0.98$
10612	7.6597	1.8	4.2	13.0	23.6	77.5	<0.36	$1.84 \pm 0.48$	$6.97 \pm 0.31$

<sup>i</sup> S/N ratio of the respective emission line.

<sup>ii</sup>  $3\sigma$  upper limit for [Ne V]  $\lambda 3427$  nondetections.

stellar+blackbody, and AGN models. We show our  $z \sim 0$ ,  $z \sim 1.6$ , and  $5 < z < 8.5$  comparison samples. We note that nearly all of the [Ne V]-emitting objects and the SMACS objects with [Ne V] limits are consistent with photoionization dominated by AGN activity by the [Backhaus et al. 2022](#) diagnostic. For maximal completeness, we require a S/N greater than 1 for the OHNO emission lines. The black hole accretion models and the NGC 5548 model show line ratios consistent with expectations for traditional AGN at high ionization parameters. We also show that extreme stellar populations are capable of producing line ratios which would be labeled as AGN by the [Backhaus et al. 2022](#) diagnostic.

#### 4.2. The Ne53 Ratio

As [Ne V] requires ionization energies much higher than those of most other strong rest-frame UV/optical emission lines (97.11-125.26 eV), it probes extremely energetic photoionization missed by lower-energy tracers. By taking the ratio of [Ne V] to lower ionization species, we can trace physical conditions of the ISM missed by other line ratios, such as [O III]/H $\beta$ , [Ne III]/[O II], [S II]/H $\alpha$  or [N II]/H $\alpha$ . We define the Ne53 ratio as

$$\text{Ne53} = \frac{[\text{Ne V}] \lambda 3427}{[\text{Ne III}] \lambda 3870} \quad (3)$$

Ne53 is an opportunistic line ratio of study for several reasons. These species of neon evolve strongly with temperature and are relatively insensitive to changes in density (see Appendix A of [Cleri et al. 2023](#)), both [Ne V] and [Ne III] are accessible to *JWST*/NIRSpec spectroscopy from  $z \sim 2$  to 12, and are close enough in wavelength for the ratio to be relatively insensitive to dust attenuation and instrumental effects such as calibration uncertainties. These two lines in particular also have the advantage of not being blended with other significant spectral features. For this reason, we choose to not use the [Ne V]  $\lambda 3347$ , [Ne III]  $\lambda 3968$ , or [Ne III]  $\lambda 3343$  lines in this ratio due to blending with each other or nearby lines at lower spectral resolutions.

The advantage of Ne53 is the large difference in minimum energy required to produce the emission lines: 97.11 eV for [Ne V] and 40.96 eV for [Ne III]. This traces the “very high” to “high” ionization zones of [Berg et al. \(2021\)](#). Ne53 also has the advantage of eliminating any abundance degeneracy from using spectral lines of two different elements.

We explore Ne53 as an indicator of black hole accretion or of the hard ionizing radiation from extreme stellar populations in Figure 5. We show a clear difference of several orders of magnitude between the AGN and BPASS/BPASS + black-body models in Ne53 space; especially interesting is that the Pop III star models are competitive with AGN in the production of [Ne V] relative to [Ne III], with the Pop III models residing a similar region of the parameters space as the low-mass ( $M_{\text{BH}} \leq 10^5 M_{\odot}$ ) black hole accretion disk models. The BPASS-only models fail to produce any meaningful [Ne V], with log(Ne53) ratios peaking around -5 for all metallicities.

We include polygons in Figure 5 to mark the general locations of different ionizing engines in this parameter space. We empirically separate the [O III]/H $\beta$  versus Ne53 diagram into four regions:

- $\log \text{Ne53} < -5$ : Objects dominated by “normal” star formation alone.
- $\log [\text{O III}]/\text{H}\beta < 1$  AND  $-5 < \log \text{Ne53} < -0.3$ : “Composite” zone of multiple potential ionizing sources.
- $(\log [\text{O III}]/\text{H}\beta > 1 \text{ AND } -5 < \log \text{Ne53} < -0.3)$  OR  $(\log [\text{O III}]/\text{H}\beta > 0.6 \text{ AND } \log \text{Ne53} > -0.3)$ : “Traditional” SMBH accretion disk AGN.
- $\log [\text{O III}]/\text{H}\beta < 0.6$  AND  $\log \text{Ne53} > -0.3$ : Pop III stars or IMBH accretion disks.

We show our photoionization models compared to our  $z \sim 0$ ,  $z \sim 1.6$ , and  $5 < z < 8.5$  samples to show that objects with well-detected [Ne V] emission are many orders of magnitude inconsistent with stellar population-only models from BPASS, even at the highest ionization parameters. We also show that the  $3\sigma$  upper limits of Ne53 place the SMACS

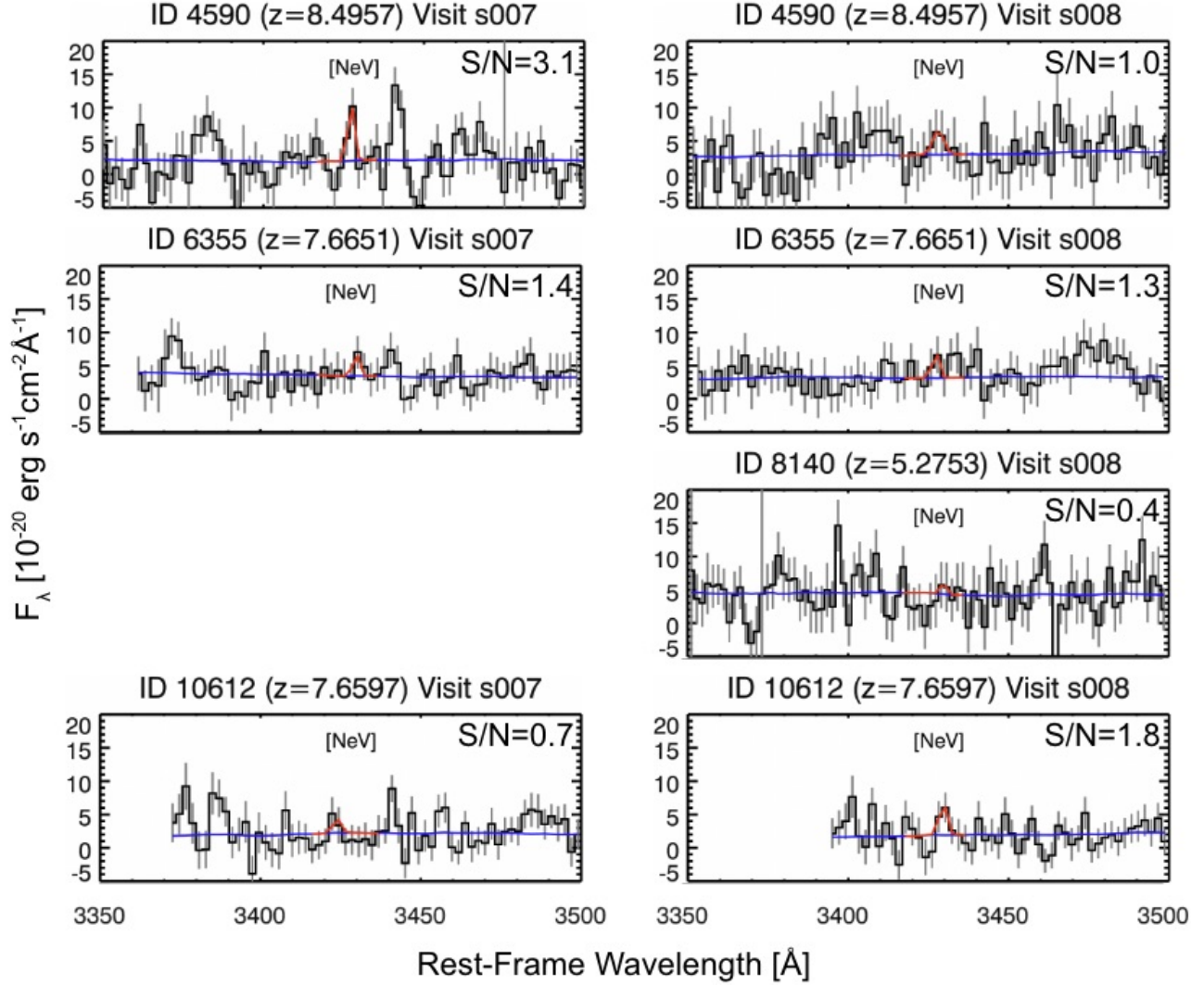


**Figure 3.** Fits to [Ne V]  $\lambda 3427$  for the four  $5.3 < z < 8.5$  SMACS ERO galaxies from the Trump et al. (2023) sample with [Ne V] coverage in *JWST*/NIRSpec. Each row shows the spectra for one object (with IDs from Trump et al. 2023 labeled) where the two panels in each row show the spectra from the two different Visits (“s007” and “s008”, respectively). The blue and red lines denote the continuum and emission line fits, respectively. We show the signal-to-noise ratio (S/N) for the fits in each visit. We do not show the first visit for ID 8140 as there is a spectral artifact at the observed wavelength of [Ne V]  $\lambda 3427$ , making an accurate line measurement impossible. We note that none of these objects are well-detected ( $S/N > 3$ ) in [Ne V] by coadded spectra between visits. The S/N ratios and relevant emission-line ratios for these objects are given in Table 1.

galaxies at  $5 < z < 8.5$  near the boundary of the Composite and AGN/Pop III/IMBH regions, but we do not draw any significant conclusions to the low S/N of these measurements.

## 5. DISCUSSION

The emission-line ratio diagnostics of Figures 4 and 5 carry many implications of the nature of EIGs and [Ne V] emission. The Ne53 ratio (see Figure 5) separates AGN and Pop III models from BPASS/BPASS + blackbody stellar models by several orders of magnitude at a given ionization parameter. As such, we conclude that the Ne53 ratio is an effective diagnostic of hard radiation fields. However, there is a large region where the Ne53 and [O III]/H $\beta$  ratios could stem from

star formation or AGN (labeled “composite” in Figure 5), but any object that resides in this region is of interest as they will be EIGs with possible indications of exotic stellar populations, accreting IMBH, or both. Therefore, Ne53 alone is not sufficient to separate AGN from extreme stellar populations, such as those presented in our Pop III models.

The OHNO diagnostic (Figure 4) shows that nearly all of the compared galaxies with [Ne V] detections (or upper limits to [Ne V] for the SMACS objects) are consistent with photoionization from an AGN, as defined by the Backhaus et al. 2022 division (Equation 2). This result shows that the OHNO diagram is not an accurate diagnostic for the most extreme emission-line galaxies in the local Universe, given our com-

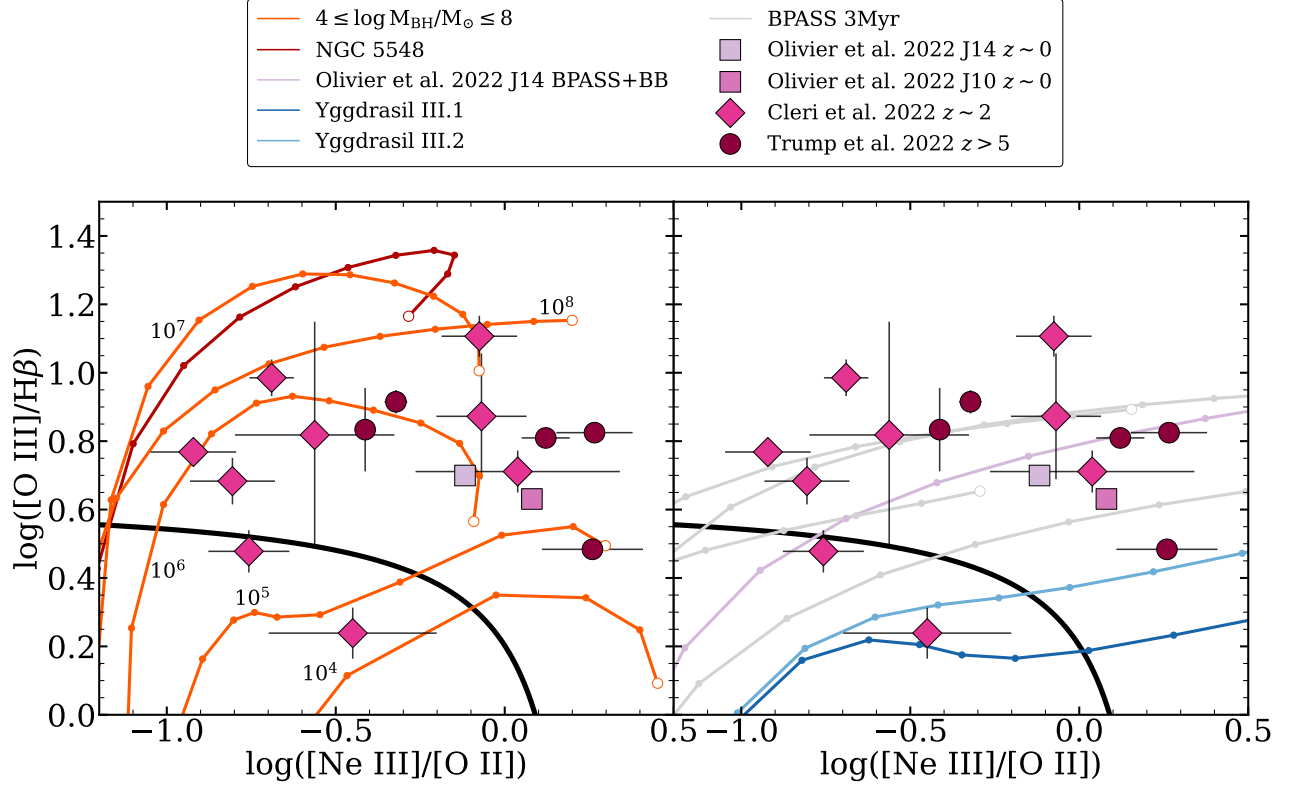


**Figure 4.** The OHNO diagram of  $\log([\text{O III}]/\text{H}\beta)$  versus  $\log([\text{Ne III}]/[\text{O II}])$ . Models are shown in a grid of dimensionless ionization parameter  $-4 \leq \log U \leq -1$ , with the open symbol at the end of each track marking  $\log U = -1$ . *Left:* AGN models in OHNO parameter space. We also show the NGC 5548 SED from Mehdipour et al. 2015 in red, and black hole accretion disk models from  $4 \leq \log M_{\text{BH}}/M_{\odot} \leq 8$  in orange, with annotations indicate the black hole mass of each model. *Right:* Stellar population models in OHNO parameter space. We show the BPASS 3 Myr stellar populations of a range of metallicities  $Z = 0.00005, 0.05, 0.10, 0.20, 0.50, 1Z_{\odot}$  in gray. We also include the Olivier et al. (2022) BPASS+blackbody model for J141851 in purple, and the Yggdrasil Population III.1 and III.2 models in dark and light blue, respectively. In each panel we show the  $z \sim 0$  data from Olivier et al. 2022,  $z \sim 2$  observations from Cleri et al. 2023, and  $z > 5$  observations from Trump et al. (2023).

parison to J141851 and J104457 from Olivier et al. 2022 and Berg et al. 2019, 2021. This is likely due to the calibration of the OHNO AGN/SF division from Backhaus et al. 2022 being based on much higher mass X-ray AGN at  $z \sim 1-2$ , and as such OHNO is not designed to discriminate AGN emission from low-mass metal-poor EIGs like J104457 and J141851.

If very high redshift galaxies are similar to the EIGs studied by Olivier et al. 2022, then the (Backhaus et al. 2022) OHNO division between AGN and star-forming galaxies may be inaccurate. As such, we do not adhere to the OHNO classifications of the SMACS ERO objects at  $z > 5$  as AGN. Other works have conjectured that a subset of these objects may be narrow-line AGN (Brinchmann 2023), but there is not conclusive evidence from other metrics for the AGN nature of any of these galaxies.

Our black hole accretion disk models for AGN cover a wide region of the OHNO parameter space. The higher black hole mass ( $M_{\text{BH}} \geq 10^6 M_{\odot}$ ) models produce higher  $[\text{O III}]/\text{H}\beta$  and lower  $[\text{Ne III}]/[\text{O II}]$  ratios than the lower black hole mass models. The higher black hole mass models are similar to the

galaxies in the  $z \sim 2$  comparison sample of  $[\text{Ne V}]$  emitting galaxies from Cleri et al. 2023, which is most similar to the Backhaus et al. 2022 sample from which the OHNO diagnostic was derived.

The photoionization models show increased  $[\text{Ne III}]/[\text{O II}]$  compared to  $[\text{O III}]/\text{H}\beta$  for AGN, along with increased  $[\text{O III}]/\text{H}\beta$  from the BPASS+blackbody models from Olivier et al. (2022). As a useful proof of concept for the variable  $M_{\text{BH}}$  accretion disk models, we note that the NGC 5548 model resides in a similar parameter space as the high-mass ( $M_{\text{BH}} \geq 10^7 M_{\odot}$ ) Done et al. (2012) models. We also note that the Pop III models occupy the lowest  $[\text{O III}]/\text{H}\beta$  but highest  $[\text{Ne III}]/[\text{O II}]$  of any of the models presented.

Other non-AGN and non-SF explanations of  $[\text{Ne V}]$  emission remain an open question. Other works have attributed  $[\text{Ne V}]$  emission in small samples of galaxies to shocks from supernovae (Izotov et al. 2012, 2021; Leung et al. 2021), but are unable to rule out production via AGN on a population level.

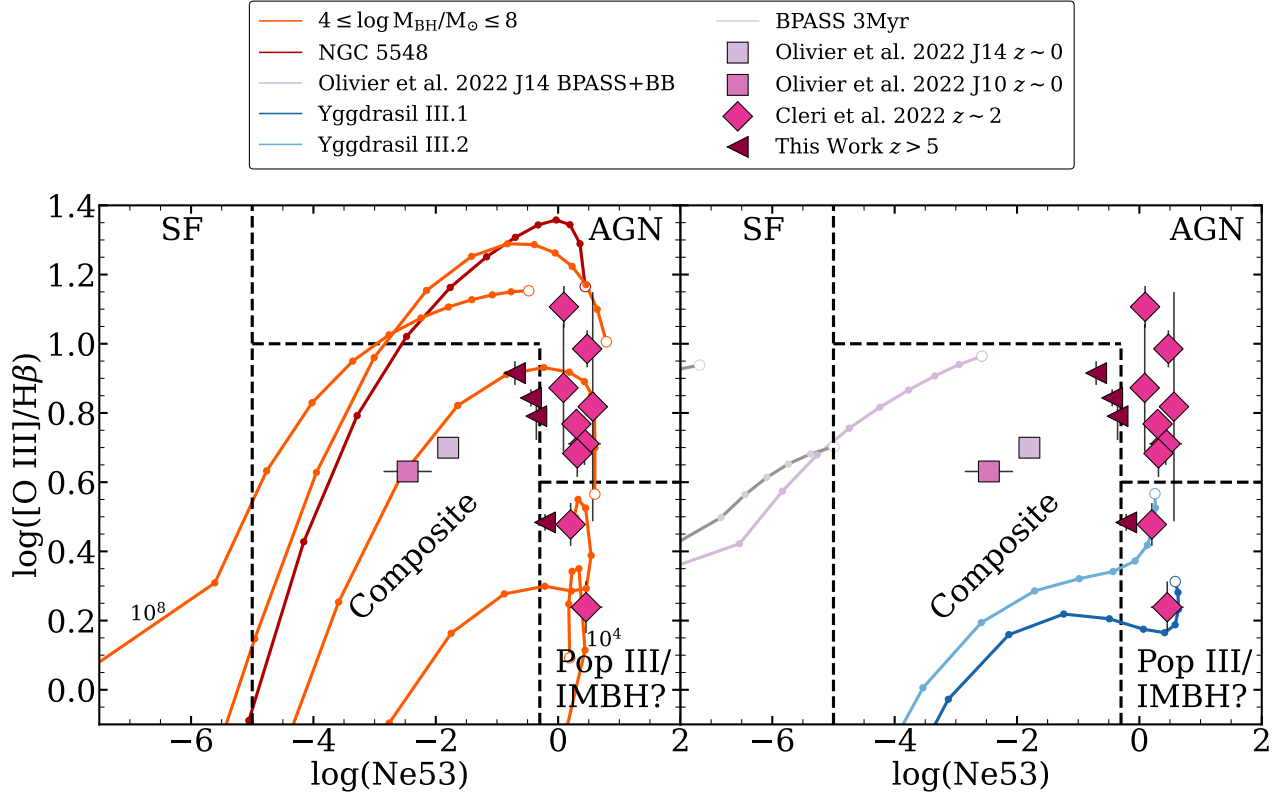


**Figure 5.** The relation between  $[\text{O III}]/\text{H}\beta$  and  $[\text{Ne V}]/[\text{Ne III}]$  (Ne53) ratios. Models are shown in a grid of dimensionless ionization parameter  $-4 \leq \log U \leq -1$ , with the open symbol at the end of each track marking  $\log U = -1$ . *Left:*  $\log([\text{O III}]/\text{H}\beta)$  versus  $\log(\text{Ne53})$  showing AGN models. We show the variable  $M_{\text{BH}}$  accretion disk models in orange, marking the extremes of  $\log M_{\text{BH}}/M_{\odot} = 8$  and  $\log M_{\text{BH}}/M_{\odot} = 4$ , and the NGC 5548 SED from Mehdipour et al. 2015 in red. *Right:*  $\log([\text{O III}]/\text{H}\beta)$  versus  $\log(\text{Ne53})$  showing stellar population models. We show the BPASS 3 Myr stellar population models in gray for metallicities  $Z = 0.00005, 0.05, 0.10, 0.20, 0.50, 1Z_{\odot}$  (most lines are off the plot left). We also include the Olivier et al. (2022) BPASS+blackbody model for the local high-ionization metal-poor dwarf J141851 in purple, and the Yggdrasil Population III.1 and III.2 models in dark and light blue, respectively. In each panel we show the  $z \sim 0$  data from Olivier et al. 2022,  $z \sim 2$  observations from Cleri et al. 2023, and  $z > 5$  observations from Trump et al. (2023) including their  $3\sigma$  upper limits on Ne53 as measured in this work. We note a distinct separation between the parameter space covered by the AGN models and the BPASS stellar populations. The BPASS models are unable to reproduce observed Ne53 ratios, even at the highest ionization parameters. The dashed black lines delineate regions where the line ratios are mostly consistent with ionization from star-formation (SF), AGN, a composite of potential SF and AGN, and possible ionization from Pop III stars or accretion onto IMBHs.

Perhaps the most intriguing alternative explanation for  $[\text{Ne V}]$  production in the early Universe is through exotic Pop III stars. While exact constraints on the nature of Pop III stars and the high-redshift IMF remain unknown, we show that current models of Pop III stars are indeed capable of providing the energetic radiation necessary to produce ultra-high ionization emission features such as  $[\text{Ne V}]$  (see Figure 5).

Throughout the analyses performed in this work, we have identified an interesting diagnostic for Pop III stars and IMBH accretion disks. The emission line ratio relations in Figures 4 and 5 can be used in conjunction to separate objects four distinct groups (see Section 4 for exact delineations):

- Objects dominated by star formation do not produce significant  $[\text{Ne V}]$ , thus lie very low (or undetectable) in Ne53 (Figure 5).
- AGN dominated by supermassive ( $M_{\text{BH}} \geq 10^6 M_{\odot}$ ) black hole accretion disks produce high  $[\text{O III}]/\text{H}\beta$  ratios, consistent with traditional star formation/AGN diagnostics (e.g., Veilleux & Osterbrock 1987; Baldwin et al. 1981; Backhaus et al. 2022).
- Objects dominated by Pop III stars or AGN with lower-mass black holes (IMBHs, with  $M_{\text{BH}} \lesssim 10^5 M_{\odot}$ ) reside in a unique parameter space in the emission line ratio relations in this work. These objects are low in  $[\text{O III}]/\text{H}\beta$ , yet high in both  $[\text{Ne III}]/[\text{O II}]$  and Ne53, similar to the parameter space occupied by the Pop III models.
- A composite region for objects which have spectra with contributions from a variety of ionizing sources.



Objects with significant contribution to their spectra from Pop III stars and lower mass black hole accretion disks are both poorly understood. Information from emission-line ratios such as those presented in this work will offer insight into the physical conditions of these interesting objects.

We look to future observations from the *James Webb Space Telescope* and next-generation facilities to offer constraints on these exotic stellar populations through emission-line spectroscopy of EIGs. Recent studies (Trussler et al. 2022) have suggested that *JWST* is capable of detecting  $M_* = 10^6 M_\odot$  Pop III galaxies at  $z \sim 8$  spectroscopically, with (very) deep integrations of tens to hundreds of hours of NIRSpec/G140M time. However, Trussler et al. (2022) calculates that moderately-lensed or more massive ( $M_* = 2 - 3 \times 10^6 M_\odot$ ) Pop III galaxies will be detectable with medium sized *JWST* General Observer programs (25-75 hours).

We caution against the general use of lower-ionization emission-line ratio diagnostics of star-formation and AGN (e.g., BPT, VO87, OHNO, etc.) for high-redshift systems as the sole discriminator between sources of ionization. In general, the use of emission-line ratio diagnostics for objects or redshift regimes for which they are not designed is questionable. Recent works have discussed the need for more emission-line ratio diagnostics which are more robust across redshifts, e.g., Figure 5 in this work. Instead, we suggest the aggregation of multiple tracers of black hole accretion/extreme stellar populations to make decisive conclusions about the nature of the ionizing spectra of high-redshift objects: emission-line velocity profiles, broad line components, multiwavelength luminosities (X-ray, radio, mid-IR, ...), etc. (see Larson et al. 2023 for a discussion of AGN tracers for the current highest-redshift AGN candidate at  $z=8.7$ ).

## 6. SUMMARY AND CONCLUSIONS

In this work, we used photoionization models to explore the physical conditions of [Ne V]  $\lambda 3427$  emission in extreme ionization galaxies (EIGs) across cosmic time. We produce Cloudy photoionization models using incident SEDs from BPASS stellar populations alone Stanway & Eldridge (2018), variable mass black hole accretion disks (Done et al. 2012; Cann et al. 2018), the well-studied local Seyfert NGC 5548 Mehdipour et al. (2015), and the Yggdrasil Population III.1 and III.2 models (Zackrisson et al. 2011). We also include the BPASS stellar populations plus an 80 kK blackbody model of local metal-poor dwarf galaxy J141851 (Olivier et al. 2022). We compare our results to observations of galaxies at  $z \sim 0$  (Berg et al. 2016, 2019, 2021; Olivier et al. 2022),  $z \sim 2$  (Cleri et al. 2023), and  $5 > z > 8.55$  (Trump et al. 2023).

The primary findings of this work are as follows:

- We fit for [Ne V] in the  $z > 5$  SMACS 0723 sample from Trump et al. 2023, and find no significant ( $S/N > 3$ ) detections in the four objects for which there is

*JWST*/NIRSpec coverage of [Ne V]. We find marginal ( $1 < S/N < 3$ ) detections in three objects (one object with  $S/N < 1$ ), which we use to assess the limiting behavior in our emission-line ratio diagnostics. We publish our measured [Ne V]  $\lambda 3427$  S/N ratios and emission-line ratios in Table 1.

- The [Ne V]/[Ne III] (Ne53) ratio is an effective indicator of photoionization from a source other than “normal” stellar populations. Current photoionization models cannot reproduce [Ne V] emission with “normal” stellar populations alone (such as those from the BPASS models, see Figure 5). We conclude that the measurement of any meaningful detection of Ne53 ( $\log \text{Ne53} \gtrsim -5$ ) likely implies the presence of an ionizing engine other than “normal” stellar populations alone (e.g., likely either AGN or Population III stars).
- We use Ne53 in conjunction with other line ratios to produce a diagnostic of AGN and Population III star activity. We propose the combination of Figures 5 and 4 to be used as such a diagnostic, where we anticipate galaxies with significant contributions of their ionizing radiation from Population III stars or low-mass AGN ( $M_{\text{BH}} \leq 10^5 M_\odot$ ) to reside in low [O III]/H $\beta$  ( $\log [\text{O III}]/\text{H}\beta \lesssim 0.6$ ) and high [Ne III]/[O II] ( $\log [\text{Ne III}]/[\text{O II}] \gtrsim 0$ ) and Ne53 ( $\log \text{Ne53} \gtrsim -0.3$ , indicating very high ionization) parameter spaces. We propose that Figure 5 can be used in future studies in conjunction with other AGN tracers (e.g., velocity profiles, broad line components, X-ray/radio/mid-IR luminosities) to further separate sources of ionizing radiation.

Our results show that [Ne V] emission probes highly energetic photoionization ( $\sim 100$  eV), which, for the models used in this work, is only reproducible by black hole accretion or Pop III stars. Although we attribute the [Ne V] production in many of the galaxies in our comparison samples, we also note that there are other production mechanisms, namely supernova shocks or other exotic stellar populations (e.g., Wolf-Rayet stars). We note that the unknown nature of Pop III stars and low-mass black hole accretion disks in the early Universe indicates that epoch of reionization galaxies are an exciting laboratory in which to study these extreme emission lines. We also note that the potential coevolution of accreting black holes and stellar populations in the early Universe can have competing contributions to the production of high-ionization emission lines. Regardless, galaxies that show strong Ne53 and low [O III]/H $\beta$  will be candidates for rare sources and may guide us to galaxies with ionization from either the first stars or AGN with lower mass black holes.

As such, these results motivate future observations of very high-ionization emission lines, like [Ne V]  $\lambda 3427$ , using

cutting-edge observatories like the *James Webb Space Telescope*. *JWST* will reach a flux limit that is an order of magnitude fainter than the *HST* data from the Cleri et al. (2023) sample for similar exposure times, enabling detection of fainter [Ne V]-line emission. *JWST* is outfitted with NIRSpec and NIRCarn, both of which had spectroscopic capabilities covering strong UV high-ionization emission lines, like the [Ne V] doublet, over a range of redshift (e.g.,  $6 < z < 11$ ). Even *JWST*/NIRISS can cover of [Ne V] at slightly lower redshift ranges ( $3 < z < 7$ ).

*JWST*/MIRI even provides low ( $R \sim 100$ ) and medium resolution ( $R \sim 1500$ -3500) spectroscopy, which covers 5–28  $\mu\text{m}$ . This will be able to observe rest-frame UV/optical spectral features for bright galaxies out to ultra-high-redshifts ( $z > 15$ ). Spectroscopy in this very early epoch in cosmic history will give direct measurements of first-generation stellar populations, as well as the beginning of chemical enrichment of the ISM.

The potential degeneracy of [Ne V] production from low-mass black hole accretion disks or Pop III stars in the early Universe is difficult to break with rest-UV/optical line ratios alone. In addition to the integrated emission-line diagnostics we present in this work (Figures 4 and 5), we can pose a solution using the integral field unit (IFU) capabilities of *JWST*/NIRSpec by looking at the spatial distribution and compactness of the high-ionization emission. We expect galaxies with significant Pop III fractions to be more uniformly distributed in their [Ne V] emission (or other very high ionization emission) than an AGN, where we expect the emission to be highly centrally dense. We can also break this degeneracy with more spectral information, including more detailed chemical abundances and metallicities.

Future studies using current and next-generation systems of high-redshift systems through the lens of extreme high-ionization emission lines, including [Ne V], will offer long-awaited answers to the underlying physics of the epoch of reionization.

**Software:** `grizli` (Brammer et al. 2008), `FAST` (Kriek et al. 2009), `EAZY` (Brammer et al. 2008; Wuyts et al. 2011), `Astropy` (Astropy Collaboration et al. 2013), `NumPy` (Harris et al. 2020), `Matplotlib` (Hunter 2007), `Cloudy` (Ferland et al. 2017), `seaborn` (Waskom 2021), `pandas` (Reback et al. 2022), `XSPEC` (Arnaud 1996)

## ACKNOWLEDGMENTS

This work is based on data obtained from the Hubble Space Telescope through program number GO-14227. Support for Program number GO-14227 was provided by NASA through a grant from the Space Telescope Science Institute, which is operated by the Association of Universities for Research in Astronomy, Incorporated, under NASA contract NAS5-26555. NJC, JRT, and BEB acknowledge support from NSF grant CAREER-1945546 and NASA grants JWST-ERS-01345 and 18-2ADAP18-0177. NJC, JRT, CP and BEB acknowledge support NASA grant JWST-ERS-01345. NJC and CP also acknowledge support from NASA/*HST* AR 16609. This work acknowledges support from the NASA/ESA/CSA James Webb Space Telescope through the Space Telescope Science Institute, which is operated by the Association of Universities for Research in Astronomy, Incorporated, under NASA contract NAS5-03127. Support for program No. JWST-ERS01345 was provided through a grant from the STScI under NASA contract NAS5-03127. TAH and AY are supported by appointments to the NASA Postdoctoral Program (NPP) at NASA Goddard Space Flight Center, administered by Oak Ridge Associated Universities under contract with NASA.

The authors thank Shobita Satyapal, Jeffrey Mckaig, and Jenna Cann for discussion and providing assistance with photoionization modeling. NJC thanks Jonathan Cohn, Justin Cole, and Maeve Curliss for insightful scientific and data visualization discussions. NJC also thanks the CANDELS Lyman- $\alpha$  Emission at Reionization (CLEAR) and Cosmic Evolution Early Release Science (CEERS) collaborations for influential discussions.

Some of the data presented in this paper were obtained from the Mikulski Archive for Space Telescopes (MAST) at the Space Telescope Science Institute. The Berg et al. (2019); Olivier et al. (2022) data can be accessed via DOI: 10.3847/1538-4357/ac8f2c. The CLEAR (Simons et al. 2023) data can be accessed via DOI: 10.3847/1538-4365/acc517. The SMACS 0723 data from Trump et al. (2023) can be accessed via DOI: 10.3847/1538-4357/acba8a.

## REFERENCES

- Adhikari, T. P., Różańska, A., Czerny, B., Hryniewicz, K., & Ferland, G. J. 2016, *ApJ*, 831, 68
- Amorín, R., Pérez-Montero, E., Contini, T., et al. 2015, *A&A*, 578, A105
- Amorín, R., Fontana, A., Pérez-Montero, E., et al. 2017, *Nature Astronomy*, 1, 0052
- Arnaud, K. A. 1996, in *Astronomical Society of the Pacific Conference Series*, Vol. 101, *Astronomical Data Analysis Software and Systems V*, ed. G. H. Jacoby & J. Barnes, 17
- Astropy Collaboration, Robitaille, T. P., Tollerud, E. J., et al. 2013, *A&A*, 558, A33
- Atek, H., Siana, B., Scarlata, C., et al. 2011, *ApJ*, 743, 121
- Backhaus, B. E., Trump, J. R., Cleri, N. J., et al. 2022, *ApJ*, 926, 161
- Baldwin, J. A., Phillips, M. M., & Terlevich, R. 1981, *PASP*, 93, 5
- Baraffe, I., & Kolb, U. 2000, *MNRAS*, 318, 354
- Bentz, M. C., Denney, K. D., Cackett, E. M., et al. 2007, *ApJ*, 662, 205
- Berg, D. A., Chisholm, J., Erb, D. K., et al. 2019, *ApJL*, 878, L3  
—, 2021, *ApJ*, 922, 170
- Berg, D. A., Skillman, E. D., Henry, R. B. C., Erb, D. K., & Carigi, L. 2016, *ApJ*, 827, 126
- Binette, L., Prieto, A., Szuszkiewicz, E., & Zheng, W. 1989, *ApJ*, 343, 135
- Brammer, G. B., van Dokkum, P. G., & Coppi, P. 2008, *ApJ*, 686, 1503
- Brinchmann, J. 2023, *MNRAS*, arXiv:2208.07467
- Bromm, V., Coppi, P. S., & Larson, R. B. 1999, *ApJL*, 527, L5
- Buat, V., Boselli, A., Gavazzi, G., & Bonfanti, C. 2002, *A&A*, 383, 801
- Cann, J. M., Satyapal, S., Abel, N. P., et al. 2018, *ApJ*, 861, 142
- Clavel, J., Boksenberg, A., Bromage, G. E., et al. 1990, *MNRAS*, 246, 668
- Cleri, N. J., Yang, G., Papovich, C., et al. 2023, *ApJ*, 948, 112
- Curtis-Lake, E., Carniani, S., Cameron, A., et al. 2023, *Nature Astronomy*, 7, 622
- Done, C., Davis, S. W., Jin, C., Blaes, O., & Ward, M. 2012, *MNRAS*, 420, 1848
- Dopita, M. A., Kewley, L. J., Heisler, C. A., & Sutherland, R. S. 2000, *ApJ*, 542, 224
- Estrada-Carpenter, V., Papovich, C., Momcheva, I., et al. 2019, *ApJ*, 870, 133  
—, 2020, *ApJ*, 898, 171
- Fan, X., Strauss, M. A., Becker, R. H., et al. 2006, *AJ*, 132, 117
- Ferland, G. J., Chatzikos, M., Guzmán, F., et al. 2017, *RMxAA*, 53, 385
- Finkelstein, S. L., Ryan, Russell E., J., Papovich, C., et al. 2015, *ApJ*, 810, 71
- Finlator, K., Keating, L., Oppenheimer, B. D., Davé, R., & Zackrisson, E. 2018, *MNRAS*, 480, 2628
- Finlator, K., Oppenheimer, B. D., Davé, R., et al. 2016, *MNRAS*, 459, 2299
- Finlator, K., Thompson, R., Huang, S., et al. 2015, *MNRAS*, 447, 2526
- Flores-Fajardo, N., Morisset, C., Stasińska, G., & Binette, L. 2011, *MNRAS*, 415, 2182
- Gierliński, M., & Done, C. 2004, *MNRAS*, 349, L7
- Gilli, R., Vignali, C., Mignoli, M., et al. 2010, *A&A*, 519, A92
- Greif, T. H., & Bromm, V. 2006, *MNRAS*, 373, 128
- Grevesse, N., Asplund, M., Sauval, A. J., & Scott, P. 2010, *Ap&SS*, 328, 179
- Groves, B., Brinchmann, J., & Walcher, C. J. 2012, *MNRAS*, 419, 1402
- Harris, C. R., Millman, K. J., van der Walt, S. J., et al. 2020, *Nature*, 585, 357. <https://doi.org/10.1038/s41586-020-2649-2>
- Heger, A., Woosley, S., Baraffe, I., & Abel, T. 2002, in *Lighthouses of the Universe: The Most Luminous Celestial Objects and Their Use for Cosmology*, ed. M. Gilfanov, R. Sunyaev, & E. Churazov, 369
- Hunter, J. D. 2007, *Computing in Science and Engineering*, 9, 90
- Inoue, A. K. 2011, *MNRAS*, 415, 2920
- Izotov, Y. I., Thuan, T. X., & Guseva, N. G. 2021, *MNRAS*, 508, 2556
- Izotov, Y. I., Thuan, T. X., & Privon, G. 2012, *MNRAS*, 427, 1229
- Katz, H., Kimm, T., Ellis, R. S., Devriendt, J., & Slyz, A. 2022, *arXiv e-prints*, arXiv:2207.04751
- Katz, H., Saxena, A., Cameron, A. J., et al. 2023, *MNRAS*, 518, 592
- Kehrig, C., Guerrero, M. A., Vílchez, J. M., & Ramos-Larios, G. 2021, *ApJL*, 908, L54
- Kehrig, C., Vílchez, J. M., Guerrero, M. A., et al. 2018, *MNRAS*, 480, 1081
- Kehrig, C., Vílchez, J. M., Pérez-Montero, E., et al. 2015, *ApJL*, 801, L28
- Kennicutt, Robert C., J. 1998, *ApJ*, 498, 541
- Kennicutt, R. C., & Evans, N. J. 2012, *ARA&A*, 50, 531
- Kewley, L. J., Nicholls, D. C., & Sutherland, R. S. 2019, *ARA&A*, 57, 511
- Korista, K., Ferland, G., & Baldwin, J. 1997, *ApJ*, 487, 555
- Kormendy, J., & Ho, L. C. 2013, *ARA&A*, 51, 511
- Kriek, M., van Dokkum, P. G., Labbé, I., et al. 2009, *ApJ*, 700, 221
- Kudritzki, R.-P. 2000, in *The First Stars*, ed. A. Weiss, T. G. Abel, & V. Hill, 127
- Larson, R. L., Finkelstein, S. L., Kocevski, D. D., et al. 2023, *arXiv e-prints*, arXiv:2303.08918
- Lequeux, J., Peimbert, M., Rayo, J. F., Serrano, A., & Torres-Peimbert, S. 1979, *A&A*, 80, 155

- Leung, G. C. K., Coil, A. L., Rupke, D. S. N., & Perrotta, S. 2021, *ApJ*, 914, 17
- Levesque, E. M., & Richardson, M. L. A. 2014, *ApJ*, 780, 100
- Maiolino, R., & Mannucci, F. 2019, *A&A Rv*, 27, 3
- Maiolino, R., Scholtz, J., Witstok, J., et al. 2023, arXiv e-prints, arXiv:2305.12492
- Maseda, M. V., van der Wel, A., da Cunha, E., et al. 2013, *ApJL*, 778, L22
- Maseda, M. V., van der Wel, A., Rix, H.-W., et al. 2014, *ApJ*, 791, 17
- Masters, D., McCarthy, P., Siana, B., et al. 2014, *ApJ*, 785, 153
- Mehdipour, M., Kaastra, J. S., Kriss, G. A., et al. 2015, *A&A*, 575, A22
- Mignoli, M., Vignali, C., Gilli, R., et al. 2013, *A&A*, 556, A29
- Mitchell, J. A. J., Done, C., Ward, M. J., et al. 2023, *MNRAS*, arXiv:2210.11977
- Nakamura, F., & Umemura, M. 2002, *ApJ*, 569, 549
- Ohkubo, T., Nomoto, K., Umeda, H., Yoshida, N., & Tsuruta, S. 2009, *ApJ*, 706, 1184
- Olivier, G. M., Berg, D. A., Chisholm, J., et al. 2022, *ApJ*, 938, 16
- Papovich, C., Simons, R. C., Estrada-Carpenter, V., et al. 2022, *ApJ*, 937, 22
- Pérez-Montero, E., Amorín, R., Sánchez Almeida, J., et al. 2021, *MNRAS*, 504, 1237
- Peterson, B. M., Denney, K. D., De Rosa, G., et al. 2013, *ApJ*, 779, 109
- Pontoppidan, K. M., Barrientes, J., Blome, C., et al. 2022, *ApJL*, 936, L14
- Raiter, A., Schaerer, D., & Fosbury, R. A. E. 2010, *A&A*, 523, A64
- Reback, J., jbrockmendel, McKinney, W., et al. 2022, pandas-dev/pandas: Pandas 1.4.2, Zenodo, vv1.4.2, Zenodo, doi:10.5281/zenodo.3509134
- Richards, G. T., Lacy, M., Storrie-Lombardi, L. J., et al. 2006, *ApJS*, 166, 470
- Rigby, J. R., Bayliss, M. B., Gladders, M. D., et al. 2015, *ApJL*, 814, L6
- Salpeter, E. E. 1955, *ApJ*, 121, 161
- Schaerer, D. 2002, *A&A*, 382, 28
- Senchyna, P., Stark, D. P., Mirocha, J., et al. 2020, *MNRAS*, 494, 941
- Senchyna, P., Stark, D. P., Vidal-García, A., et al. 2017, *MNRAS*, 472, 2608
- Simons, R. C., Papovich, C., Momcheva, I., et al. 2021, *ApJ*, 923, 203
- Simons, R. C., Papovich, C., Momcheva, I. G., et al. 2023, *ApJS*, 266, 13
- Smit, R., Bouwens, R. J., Labbé, I., et al. 2014, *ApJ*, 784, 58
- Stanway, E. R., & Eldridge, J. J. 2018, *MNRAS*, 479, 75
- Stark, D. P. 2016, *ARA&A*, 54, 761
- Steidel, C. C., Rudie, G. C., Strom, A. L., et al. 2014, *ApJ*, 795, 165
- Tan, J. C., & McKee, C. F. 2004, *ApJ*, 603, 383
- Tang, M., Stark, D. P., Chevallard, J., & Charlot, S. 2019, *MNRAS*, 489, 2572
- Tang, M., Stark, D. P., Chevallard, J., et al. 2021, *MNRAS*, 501, 3238
- Trump, J. R., Sun, M., Zeimann, G. R., et al. 2015, *ApJ*, 811, 26
- Trump, J. R., Arrabal Haro, P., Simons, R. C., et al. 2023, *ApJ*, 945, 35
- Trussler, J. A. A., Conselice, C. J., Adams, N. J., et al. 2022, arXiv e-prints, arXiv:2211.02038
- Tumlinson, J. 2006, *ApJ*, 641, 1
- van der Wel, A., Straughn, A. N., Rix, H. W., et al. 2011, *ApJ*, 742, 111
- Vanden Berk, D. E., Richards, G. T., Bauer, A., et al. 2001, *AJ*, 122, 549
- Veilleux, S., & Osterbrock, D. E. 1987, *ApJS*, 63, 295
- Walter, R., & Fink, H. H. 1993, *A&A*, 274, 105
- Waskom, M. 2021, *The Journal of Open Source Software*, 6, 3021
- Wuyts, S., Förster Schreiber, N. M., Lutz, D., et al. 2011, *ApJ*, 738, 106
- Zackrisson, E., Rydberg, C.-E., Schaerer, D., Östlin, G., & Tuli, M. 2011, *ApJ*, 740, 13
- Zeimann, G. R., Ciardullo, R., Gebhardt, H., et al. 2015, *ApJ*, 798, 29
- Zheng, W., Kriss, G. A., Telfer, R. C., Grimes, J. P., & Davidsen, A. F. 1997, *ApJ*, 475, 469